$[Pt(phen)_2]Cl_2$ and $[Pt(bpy)_2]Cl_2$, we propose that a band is formed from the interaction of the bipyridines and not the platinums in the linear chain of $Pt(bpy)(CN)_2$ formed at the surface and that the chain is stabilized by partial reduction of the bipyridine π^* (redox orbital) band.

The question of the origin of the emissive state has been examined by Biederman et al.[9] For a single oriented crystal (where the x axis is along the linear chain), the presence of a very intense x-polarized absorption beginning at $\sim$18 000 cm^{-1} was noted. The intensity of the transition resulted in an off-scale signal above 19 000 cm^{-1} (complete absorption of incident radiation). Their polarized, temperature dependent emission studies for the C_{2V} linear chain crystal indicate that although the strong visible absorption is polarized along the linear chain axis (x, b_1), the room-temperature emission is polarized perpendicular to the crystal axis (y, b_2 or z, a_1). They proposed a singlet absorption involving promotion from a $d_{z^2-y^2}$ orbital of a_1 symmetry to an orbital of b_1 symmetry that involves a Pt $6p_x$ orbital strongly mixed with a CN π^* orbital. This would give rise to a $^1B_1$ state that would be predicted to be polarized along the crystal axis. The emissive state was assigned as the corresponding $^3B_1$ state, which is polarized perpendicular to the linear chain axis (x) due to spin-orbital coupling, which removes the triplet spin degeneracy giving A_1', A_2', and B_2' spin–orbit states.

In their analysis, they assumed that the crystal structure was similar to that of $Pt(bpy)Cl_2$, with the bpy's in a trans configuration and a Pt–Pt distance of 3.4 Å. However, as the recent X-ray structure determined by Che and co-workers[8] indicates, the bpy's are in a cis (face-to-face) configuration and the molecular interaction between $Pt(bpy)(CN)_2$ moieties is greater than that for $Pt(bpy)Cl_2$, as evidenced by the slightly shorter Pt–Pt distance (3.3 Å). Another assumption made in assigning the involved states was that the CN π^* orbitals are much lower in energy than the bpy π^* orbitals, and thus π_{bpy}–d_{Pt} orbital interaction could be neglected. However, our electrochemical results are consistent with the first reduction of $Pt(bpy)(CN)_2$ being localized in a bpy π^* orbital, thus, suggesting it as the lowest unoccupied molecular orbital (LUMO). In addition, assuming that our linear chain structure at the electrode surface is similar to that of the crystal, the RR data of the $Pt(bpy)(CN)_2$ linear chains at a platinum electrode surface indicate that the molecular distortion that occurs upon excitation of the low-energy visible transition involves only bipridine modes. On the basis of these new data, the intense absorption in the visible portion of the spectrum must involve a bpy orbital, the likely candidate being the redox orbital (b_1). Thus, the absorbing state is either ligand centered (LC, $\pi\pi^*$) or MLCT in nature.

The emitting state then is also probably LC or MLCT in nature. Most LC emissions show vibronic structure even at room temperature, and no structure is evident for the $Pt(bpy)(CN)_2$ crystal. The symmetric and antisymmetric combinations of such orbitals would result in a_1 and b_1 orbitals, respectively. Thus for interacting π orbitals, the highest occupied π^* orbital would be of b_1 symmetry, and the lowest unoccupied π^* orbital would have a_1 symmetry. The lowest energy spin-allowed state arising from these orbitals would then be a $^1B_1$ which would be x polarized (along the chain axis). In addition, the extinction coefficient for a $\pi \rightarrow \pi^*$ transition would be predicted to be very large. The highest occupied molecular orbital (HOMO) involved in this transition (b_1) would be antibonding with respect to the adjacent bipyridines in the chain, and the LUMO (a_1) would be bonding in nature with respect to the adjacent bipyridines. Upon formation of the excited state then, the bonding interaction between the bpy's would increase giving rise to an excimeric interaction similar to that postulated[3] for both $[Pt(bpy)_2]Cl_2$ and $[Pt(phen)_2]Cl_2$. Emission from excimers gives broad unstructured bands, such as the one observed. Since the corresponding emitting state would be a $^3B_1$, the fact that the emission is polarized would arise from spin–orbital coupling removing the spin degeneracy and giving rise to A_1', B_2', and A_2' spin–orbit states.

Reactant Segregation in the Steady-State A + B → 0 Reaction on Surfaces

O. M. Becker, M. Ben-Nun, and A. Ben-Shaul*

Department of Physical Chemistry and The Fritz Haber Research Center for Molecular Dynamics,
The Hebrew University, Jerusalem 91904, Israel (Received: July 30, 1990)

The steady-state bimolecular annihilation reaction A + B → 0 on two-dimensional surfaces is studied via computer simulations. In the simulations A and B are randomly adsorbed on vacant sites, and reaction takes place whenever A and B reach nearest-neighbor sites, either directly following adsorption or through diffusion. It is found that both with and without diffusion the reactants segregate into separate islands of A's and B's. The islands vary in size and exhibit highly ramified shapes. Moreover, the islands are self-similar with a fractal dimension $D = 1.89$ (similar to percolation, but also other clusters). D is found to be independent of the diffusion rate K. Other fractal dimensions, e.g., of the "hull" differ from those of percolating clusters. The steady-state coverage $\theta^* = \theta^*_A + \theta^*_B$ decreases with K, as expected ($\theta^*_A = \theta^*_B$, corresponding to equal fluxes of A and B is the only physical solution). For systems with immobile particles ($K = 0$) we find $\theta^* \cong 0.59$ and $\theta^* \cong 0.49$ for the square and the triangular lattices, respectively, similar to the percolation thresholds on these lattices. The long-time characteristics of the system (D, θ^*, etc.) are independent of the initial conditions of the simulation, indicating that the system reaches a stable steady state. Furthermore, for the large systems simulated (typically 500 × 500 lattice sites) it was found that the long-time behavior is independent of the input mode. Namely, the same results are obtained for conserved (i.e., exactly balanced) and nonconserved (statistically balanced) A,B input mechanisms, indicating that on the time scale of the simulations ($\sim 10^4$ Monte Carlo steps) the apparent steady state (for nonconserved input) is essentially identical with the true steady state (for the conserved input).

1. Introduction

The bimolecular annihilation reaction A + B → 0 is of great interest in chemical kinetics[1] as well as in various physical and biological systems. In particular, if A and B represent adsorbates on a solid surface and 0 stands for a rapidly desorbing product, the annihilation reaction above corresponds to a simple bimolecular catalytic reaction. The rates of such reactions depend critically on various factors such as the mode (e.g., "pulsed" vs "continuous") and rate of reactant input to the system, adsorbate mobilities, lateral interactions, and reaction probabilities. These factors combine to determine the spatial and temporal characteristics of the A,B overlayer on the surface. Quite often in these systems, local fluctuations in A and B densities can develop into long-range ("mesoscopic") segregation and, consequently, to marked devia-

0022-3654/91/2095-4803$02.50/0 © 1991 American Chemical Society

tions from classical ("mean field") reaction rate laws.[1-15] For catalytic surface reactions this means deviations from the simple rate law $R \sim \theta_A\theta_B$, with θ_A and θ_B denoting two-dimensional densities (coverages).[16-23] It should be noted that in many surface reactive systems reactant aggregation and segregation and consequently deviations from classical kinetics are due to adsorbate lateral interactions[23-27] and/or nonrandom adsorption mechanisms.[23,27,28] However, in this paper we are exclusively concerned with the segregation induced by the reactive process itself, i.e., by the fact that A and B react immediately whenever they are at close proximity. This process leads to nonuniform spatial distributions of the reactive adsorbates, even in noninteracting systems governed by a random adsorption mechanism.

The general conditions for reactant segregation and the causes for anomalous kinetics in the $A + B \rightarrow 0$ (and other, e.g., $A + B \rightarrow A$ or $A + A \rightarrow 0$) reactions have been the subject of intensive theoretical research in recent years.[1-15] Many of the relevant studies, which include both computer simulations and analytical approaches, consider the $A + B \rightarrow 0$ reaction in arbitrary dimensionalities, both Euclidean and fractal. Some analyses suggest the existence of a critical dimension, d_c, such that segregation takes place only for $d < d_c$. The values predicted for d_c vary with initial conditions (reaction scheme) and other parameters.[1-4,11-15]

The two commonly studied reaction schemes are termed "transient" (or pulsed) and "steady state" (or continuous). In the first case, A and B particles are created at $t = 0$ and one follows the spatial–temporal evolution of their densities.[2-7] For diffusion-limited reactions particle segregation and nonclassical lone-time behavior[2-4] characterize the system in $d < d_c = 4$. A different behavior was recently reported for the transient reaction with immobile particles reacting via exchange (exponentially decreasing with distance) probability.[15] In this case there is no upper critical dimension to segregation and nonclassical kinetics is predicted for all d.

In the steady-state reaction scheme A and B particles are continuously added to the system, with a given rate and a given spatial distribution.[9-14] Theoretical analyses[13,14] based on continuous stochastic rate equations suggest that, for diffusion-limited reactions in infinite systems, macroscopic segregation occurs for $d < 3$ and not for $d > 3$. $d = 3$ is "marginal" in the sense that the segregation behavior depends on a subtle interplay between several parameters, mainly between the diffusion and reaction rates. For finite systems the marginal dimension[13] is $d = 2$. Correlations between the added reactants can also affect the steady-state behavior in these systems.[13,14]

In this paper we are specifically interested in the steady state $A + B \rightarrow 0$ reaction in $d = 2$. As noted earlier, this is a model system, albeit idealized, for heterogeneously (surface) catalyzed reactions. More complex reactive systems (corresponding e.g. to the scheme $O_2(g) \rightarrow 2O(s)$, $CO(g) \rightarrow CO(s)$, $O(s) + CO(s) \rightarrow CO_2(g)$; g = gas, s = surface) have recently been studied via computer simulations and rate equation approaches, revealing interesting kinetic phase transitions and reactant segregation behavior.[16-22] In these systems, as well as in the simpler case[21-23] of $A + B \rightarrow 0$, segregation takes place both with and without particle diffusion. The basic driving force for segregation is the "infinite repulsion" (annihilation) between A and B on neighboring sites. Since reaction takes place at the boundaries of the segregated reactant islands, it is clear that their rates are very sensitive to the structure of these islands. Yet, the amount of information on the adlayer structure under steady-state conditions is very limited.[21-23] The most significant finding in this context, based on a simulation study by Ziff and Fichthorn[21] for a system with immobile reactants, is that the clusters of A's and B's formed in the course of reaction are self-similar, with fractal dimension $D \simeq 1.9$.

In an attempt to better understand the structural–temporal behavior of the steady-state $A + B \rightarrow 0$ reaction, we present in the following section a series of computer simulations of this system, with and without particle diffusion. As we shall see, this apparently simple reaction exhibits interesting and rather complex behavior and presents some nontrivial and puzzling questions. For example, it is clear that if steady state is achieved the rate of reaction R must be equal to the rate of particle replenishment, Q. The latter is proportional to the fraction of empty sites, hence $R = Q \sim (1 - \theta^*)$ with $\theta^* = \theta^*_A + \theta^*_B$ denoting the total steady-state coverage. On the other hand, it is not at all clear what determines θ^* and, furthermore, whether our finding that θ^* is very close to the percolation threshold on the lattices studied is physically meaningful or perhaps fortuitous.

2. Results and Discussion

In this section we present the results of computer simulations of the steady-state $A + B \rightarrow 0$ reaction, with and without reactant diffusion. A and B particles were added, with equal probabilities and randomly to the empty sites of a two-dimensional lattice. We denote by J_A the flux of A's on the surface, that is, the number of A's impinging, on the average, on one lattice site in unit time. Particles impinging on occupied sites are reflected to the gas phase. For the sticking probability of A's and B's on empty sites we take $S_A = S_B = 1$, so that J_A is also the rate of A adsorption on the bare surface. On the partly covered surface the adsorption rate of A is $J_A(1 - \theta)$. The total adsorption rate is $J(1 - \theta)$ with $J = J_A + J_B$. Reaction, i.e., AB annihilation, takes place instantaneously whenever A and B happen to occupy nearest-neighbor (nn) sites on the lattice. In simulations without diffusion, reactive events occur only if a newly added A lands next to a site occupied by B, or vice versa. If the empty site into which A has landed has more than one nn site occupied by B, one of these B's is chosen randomly to react with A, etc. It should be noted that if the rates of A and B adsorption are different the surface will be eventually

---

(1) For reviews, see e.g.: Kuzovkov, V.; Kotomin, E. *Rep. Prog. Phys.* **1988**, *51*, 1479. Gösele, U. M. *Prog. React. Kinet.* **1984**, *13*, 63.

(2) Ovchinnikov, A.; Zeldovich, Ya. B. *Chem. Phys.* **1978**, *28*, 215.

(3) Toussaint, D.; Wilczek, F. *J. Chem. Phys.* **1983**, *78*, 2642.

(4) Kang, K.; Redner, S. *Phys. Rev. Lett.* **1984**, *52*, 955.

(5) Zumofen, G.; Blumen, A.; Klafter, J. *J. Chem. Phys.* **1985**, *82*, 3198. Bromson, M.; Lebowitz, J. L. *Phys. Rev. Lett.* **1988**, *61*, 2397.

(6) Meakin, P.; Stanley, H. E. *J. Phys. A: Math. Gen.* **1984**, *17*, L173.

(7) Argyrakis, P.; Kopelman, R. *Phys. Rev. A.* **1990**, *41*, 2121.

(8) Anacker, L. W.; Kopelman, R. *J. Chem. Phys.* **1984**, *81*, 6402; *Phys. Rev. Lett.* **1987**, *58*, 289. Anacker, L. W.; Parson, R. P.; Kopelman, R. *J. Phys. Chem.* **1985**, *89*, 4758.

(9) Newhouse, J. S.; Kopelman, R. *J. Chem. Phys.* **1986**, *85*, 6804; *Phys. Rev. B* **1985**, *31*, 1677; *J. Phys. Chem.* **1988**, *92*, 1538.

(10) Anacker, L. W.; Kopelman, R. *J. Phys. Chem.* **1987**, *91*, 5555.

(11) Kanno, S. *Prog. Theor. Phys.* **1988**, *79*, 721.

(12) Zhang, Y.-C. *Phys. Rev. Lett.* **1987**, *59*, 1726.

(13) (a) Lindenberg, K.; West, B. J.; Kopelman, R. *Phys. Rev. Lett.* **1988**, *60*, 1777. (b) West, B. J.; Kopelman, R.; Lindenberg, K. *J. Stat. Phys.* **1989**, *54*, 1429. (c) Clément, E.; Sander, L. M.; Kopelman, R. *Phys. Rev. A* **1989**, *39*, 6466.

(14) (a) ben-Avraham, D.; Doering, C. R. *Phys. Rev. A* **1988**, *37*, 5007. (b) ben-Avraham, D.; Redner, S.; Considine, D. B.; Meakin, P. *J. Phys. A: Math. Gen.* **1990**, *23*, L613.

(15) Schnörer, H.; Kuzovkov, V.; Blumen, A. *Phys. Rev. Lett.* **1989**, *63*, 805; *J. Chem. Phys.* **1990**, *92*, 2310.

(16) Ziff, R. M.; Gulari, E.; Barshad, Y. *Phys. Rev. Lett.* **1986**, *56*, 2553.

(17) Wicke, F.; Kummann, P.; Keil, W.; Schiefler, J. *Ber. Bunsen-Ges. Phys. Chem.* **1980**, *84*, 314.

(18) Dickman, R. *Phys. Rev. A* **1986**, *34*, 4246.

(19) Kaukonen, H.-P.; Nieminen, R. M. *J. Chem. Phys.* **1989**, *91*, 4380. Fischer, P.; Titulaer, U. M. *Surf. Sci.* **1989**, *221*, 409. Cordoba, A.; Lemos, M. C.; Luque, J. J. *J. Chem. Phys.* **1990**, *92*, 5636.

(20) Mai, J.; von Niessen, W.; Blumen, A. *J. Chem. Phys.* **1990**, *93*, 3685.

(21) Ziff, R. M.; Fichthorn, K. *Phys. Rev. B* **1986**, *34*, 2038.

(22) Meakin, P.; Scalapino, D. J. *J. Chem. Phys.* **1987**, *87*, 731.

(23) Becker, O. M.; Silverberg, M.; Ben-Shaul, A. *Isr. J. Chem.* **1990**, *30*, 179.

(24) See, e.g.: Engel, T.; Ertl, G. *Adv. Catal.* **1978**, *28*, 1. Gland, J. L.; Kollin, E. B. *J. Chem. Phys.* **1983**, *78*, 963. Stuve, E. M.; Madix, R. J.; Brundle, C. *Surf. Sci.* **1984**, *146*, 155.

(25) Silverberg, M.; Rebentrost, F.; Ben-Shaul, A. *J. Chem. Phys.* **1985**, *83*, 6501. Silverberg, M.; Ben-Shaul, A. *J. Chem. Phys.* **1987**, *87*, 3178; *Surf. Sci.* **1989**, *214*, 43. See also *J. Stat. Phys.* **1988**, *52*, 1179.

(26) Hellsing, B.; Zhdanov, V. P. *Chem. Phys. Lett.* **1988**, *147*, 613. Gupta, D.; Hirtzel, C. S. *Mol. Phys.* **1989**, *68*, 583.

(27) Hood, E. S.; Toby, B. H.; Weinberg, W. H. *Phys. Rev. Lett.* **1985**, *55*, 2437.

(28) Becker, O. M.; Ben-Shaul, A. *Phys. Rev. Lett.* **1988**, *61*, 2859. Becker, O. M. To be published.

"poisoned" by the majority species and the reaction will terminate (see section 3). Consequently, in all our simulations we set $J_A = J_B = J/2$. In some cases this was ensured by exact balancing, i.e., by adding simultaneously "pairs" of A and B into different, randomly chosen vacant sites. In some simulations the added particle was randomly chosen (with equal probabilities for A and B), thus allowing a certain degree of density fluctuations. These two types of input may be referred to as "conserved" (or "exactly balanced") and "nonconserved" (or "statistically balanced"), respectively.[13,14] We shall compare the two mechanisms and discuss their consequences with respect to the steady-state behavior in section 2A.

In a lattice of M sites with $\theta_A M$ of its sites occupied by A's and $\theta_B M$ by B's the number of vacant sites is $M(1 - \theta_A - \theta_B) = M(1 - \theta)$. Thus, for a constant total flux $J = J_A + J_B$ there will be $JM(1 - \theta)$ adsorption events or, equivalently, JM adsorption attempts per unit time. As the unit of time in our simulations we take the time between successive adsorption attempts per lattice site; this equals $1/J$. Thus, on a lattice of M sites this time unit (hereafter 1 MCS = one Monte Carlo step) corresponds to M adsorption attempts, of which $M(1 - \theta)$ are successful. As noted above, at steady state this also means $M(1 - \theta)/2$ reactive events per MCS.

In simulations with mobile particles the computational procedure is as follows. Following every adsorption trial (i.e., randomly choosing a site and, if empty, populating it with either A or B with equal probability) we perform K diffusion trials. Each diffusion trial corresponds to randomly choosing a site, and if this site is occupied by either A or B, the particle is randomly moved into one of its vacant nn sites, provided such nn sites are available. Otherwise, the diffusion trial is rejected. This is repeated K times per adsorption trial. (Note that the probability that a diffusion trial will be successful depends on the immediate neighborhood of the particle.) If following a diffusive jump A(B) becomes a nn of B(A), reaction takes place immediately. As in diffusion-limited reactions K may be interpreted as the hopping frequency of an isolated particle, which is simply proportional to the (low density) diffusion constant. To summarize, in general, each MCS consists of $M(K + 1)$ microtrials, which include M adsorption trials ($M(1 - \theta)$ successful) and MK diffusion trials of which, at most, $MK\theta$ can be successful, because some particles are fully surrounded by (like) particles.

The majority of the simulations reported below were carried out on 500 × 500 square lattices, with periodic boundary conditions. For good statistics the results were averaged, for each initial condition, over many runs (typically 35 without diffusion, and 10 with diffusion). Several cases were also simulated on smaller square lattices, and on triangular lattices (of 250 000 sites) with periodic boundary conditions, primarily for comparative purposes. All the calculations were performed on a Silicon Graphics workstation.

2.A. Steady-State Behavior. Figure 1 shows a typical snapshot of the A,B overlayer after 2000 MCS for a system with immobile reactants ($K = 0$). The structure is dynamical, in the sense that particles are created and destroyed continuously, and the A and B clusters appear to form, disappear, coalesce, and diffuse on the surface. Snapshots of the surface at earlier and later times show very similar qualitative features, i.e., highly irregular islands of A and B, characterized by ramified boundaries and separated by a highly tortuous connected region ("buffer zone") of vacant sites. A more quantitative analysis of the overlayer, based on the calculation of structural characteristics such as the fractal dimensionality of the islands, their perimeters, and their size distributions (section 2.C), indicates that after ~10 000 MCS the system has essentially reached a steady state.

The results shown in Figure 1 correspond to a simulation in which A and B are added to an initially empty surface. It has been suggested elsewhere[22] that, even after ~10^4 MCS, the system may still be evolving toward a more segregated state. One rather straightforward test of this hypothesis would be to start the simulation from a very different initial state. The opposite extreme of the empty surface would be one in which the A and B particles are fully segregated into few (say two) large domains with smooth boundaries, with a narrow (one site wide) buffer zone separating them. We have thus carried out several simulations starting with such a precovered surface as an initial state. (A picture of this state is shown in ref 23.) It was found that the adlayer structure developing from this initial condition is very similar to the one evolving from an initially empty surface. In other words, the overlayer structure at steady state has lost all memory of the initial state.

The similarity between the long-time overlayer characteristics corresponding to the markedly different initial conditions is not only qualitative. In particular, the total coverage, $\theta = \theta_A + \theta_B$, approaches in both cases the same value $\theta^* = \theta(t \rightarrow \infty) = 0.585 \pm 0.005$, as shown in Figure 2. We are thus led to conclude that the system tends to approach a stable steady state, characterized by constant θ^* and other time-independent parameters.

It should be noted that, in a finite system, a stable or "true" steady state is achieved only for the conserved input mechanism; that is, when the A and B coverages are exactly balanced at all times (i.e., $|\theta_A - \theta_B| \equiv 0$). On the other hand if A and B are only statistically balanced (a nonconserved input mechanism), there is always a certain probability that a fluctuation in $|\theta_A - \theta_B|$ will be amplified to such an extent that the surface will be poisoned by one of the species.[13,14] It is expected that the probability of such a fluctuation will increase as the system size decreases. Alternatively, the time required for such a fluctuation should increase with the system size. In a very recent paper, ben-Avraham et al.[14b] have shown that the poisoning time in the A + B → 0 system varies as a power law of the system size L. Thus, in a finite system with nonconserved A,B input the only true steady state at $t \rightarrow \infty$ is a poisoned surface (either $\theta_A = 1$ or $\theta_B = 1$).

Most of our simulations were carried out for nonconserved input, for systems of size $L \times L = 500 \times 500$. On the time scale of the simulations, ~10^4 MCS, we have not observed surface poisoning. (A few simulations, on small systems, revealed that indeed a nonconserved input ends up with surface poisoning.) Furthermore, and more significantly, we found that the *apparent* steady state reached in these systems is the same as the *true* steady state observed in the corresponding system simulated with a conserved input mechanism. This behavior was observed in a number of cases tested. This conclusion is not very surprising for the following reason. As long as (in the nonconserved input simulations) θ_A and θ_B are nearly the same, and $\theta = \theta_A + \theta_B$ is constant and significantly less than 1 (e.g., 0.59 for the square lattice) the system is far from the poisoned state. Small fluctuations around these values, reflecting fluctuations in the A,B source, are expected to be washed out rapidly (in a large system), and the behavior resembles that of a system with conserved input. A large fluctuation, whose probability decreases with L, is required to take the system all the way to poisoning. To conclude, the apparent steady state in the nonconserved system is an excellent approximation to the true steady state in the conserved system.

The value of θ^* obtained for the square lattice is just slightly lower than the percolation threshold on this lattice, $P_c = 0.593$. The A and B clusters at steady state are large, but not infinite. Recall also that Ziff and Fichthorn[21] found $D \cong 1.9$ for the A,B clusters which is the same as the fractal dimension of percolating clusters, $D = 1.896$. (We find a similar value, see section 2C.) Lacking a theoretical explanation of this puzzling resemblance, we decided to study the A + B → 0 reaction on an additional lattice, the triangular lattice. Here we found that the steady-state coverage is $\theta^* \simeq 0.49$, again just slightly below the percolation threshold on the 2D triangular lattice, $P_c = 0.5$. Furthermore, the fractal dimension found here, $D \simeq 1.88$, appears to be the same as on the square lattice (as is rigorously the case in the percolation problem). In section 2C we compare additional characteristics of the A,B and percolation clusters, revealing some significant differences between the two types of aggregates.

2.B. Adlayer Segregation. There is more than one way to characterize the segregation of A and B. In some of the analytical studies based on continuum equations the common measure of segregation is the order parameter $S = \langle S(\mathbf{r}) \rangle$ with $S(\mathbf{r}) = [\rho_A(\mathbf{r})$

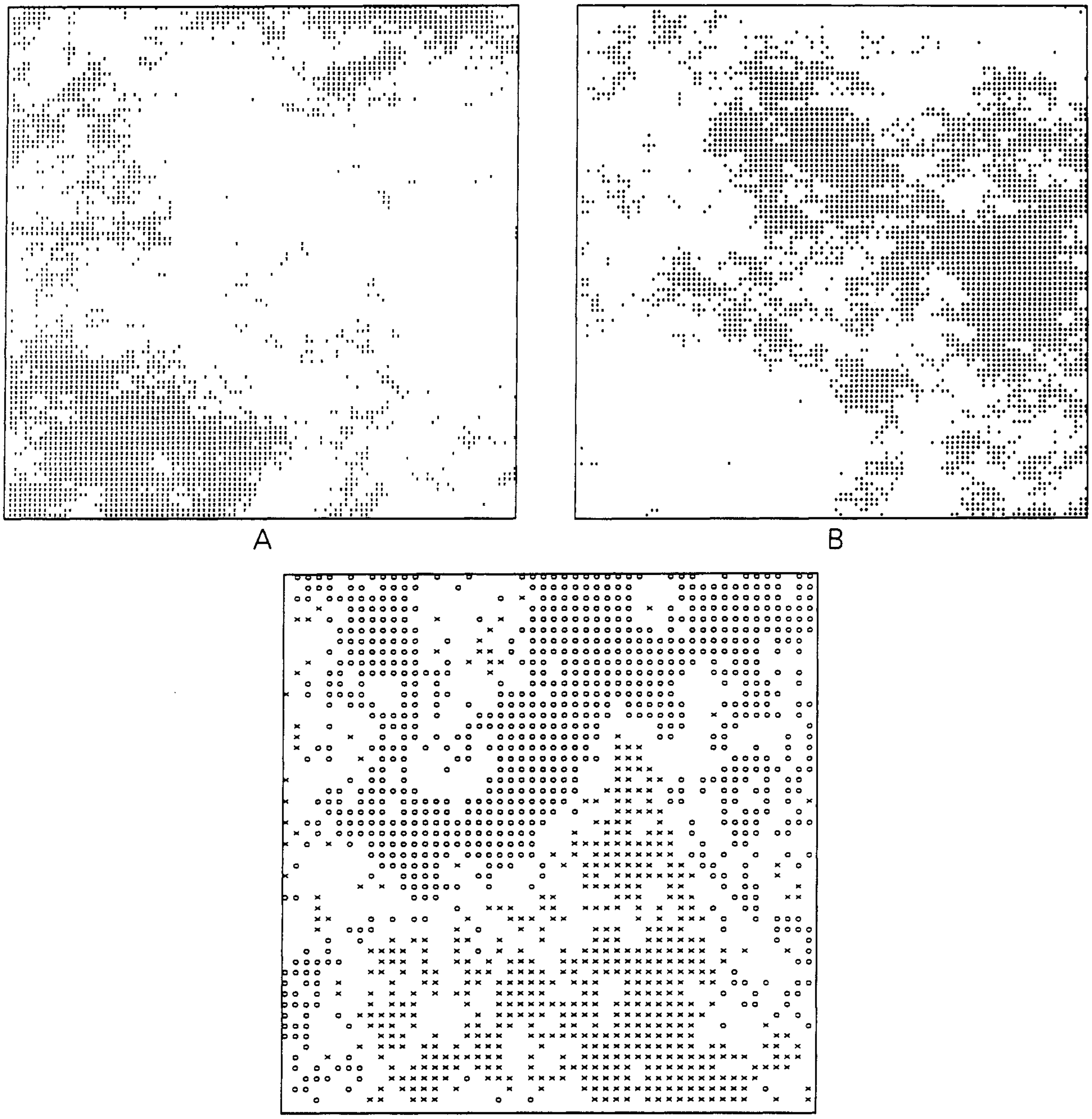

Figure 1. A snapshot of the A,B overlayer, after 2000 MCS, generated by the A + B → 0 annihilation reaction under constant impingement flux and with immobile reactants ($K = 0$). Top: A 100 × 100 section of the 500 × 500 square lattice used in the calculation, with the distributions of A's and B's separated for clarity. Bottom: A smaller section (50 × 50) of the same lattice showing both reactants simultaneously.

$-\rho_B(\mathbf{r}))^2/[\rho_A(\mathbf{r}) + \rho_B(\mathbf{r})]^2$ and $\rho_A(\mathbf{r})$ denoting the local density of A particles around $\mathbf{r}$. This measure is less convenient for lattice simulations since $S(\mathbf{r})$ will be sensitive to the extent of "coarse graining" the lattice.

As an alternative measure of the tendency of A and B to segregate we have calculated the radial distribution functions

$$g_{kl}(r) = \frac{1}{\theta_k\theta_l}\langle \rho_k(\mathbf{r}_i)\,\rho_l(\mathbf{r}_j)\rangle \qquad (1)$$

Here, k = A,B and l = A,B and $r = |\mathbf{r}_i - \mathbf{r}_j|$ is the distance between lattice sites i and j. The local coverages are calculated using $\rho_k(\mathbf{r}_i) = \delta_k(\mathbf{r}_i)$, i.e., $\rho_k(\mathbf{r}_i) = 1$ if the lattice site at $\mathbf{r}_i$ is populated by a particle of type k and 0 otherwise. Analysis of our simulation data for a 500 × 500 square lattice (and immobile adsorbates) yields for $g_{AA}(r)$ and $g_{AB}(r)$ the results displayed in Figure 3. As expected, g_{AA} and g_{AB} reveal complementary behavior. At short distances $g_{AA} > 1$ and $g_{AB} < 1$, demonstrating the tendency of like particles to aggregate and unlike particles to separate. Both g_{AA} and g_{AB} approach 1, indicating total loss of correlation when $r \gtrsim 60$ lattice units.

Another measure of the aggregation tendency in the system is provided by a familar quantity from percolation theory.[29] The connectivity (or correlation) length, ξ, defined via

$$\xi^2 = \sum_s R_s^2 s^2 n_s / \sum s^2 n_s \qquad (2)$$

where n_s is the fraction of clusters of size s (hence sn_s is the probability that a randomly chosen site belongs to a cluster of size s). R_s is the radius of gyration of a cluster of size s

$$2R_s^2 = \sum_{i,j} (\mathbf{r}_i - \mathbf{r}_j)^2/s^2 \qquad (3)$$

with the sum extending over all pairs of sites belonging to the s cluster. Note that $2R_s^2$ is the average square distance between two cluster sites. Since sn_s is the probability that a given site

---

(29) See, e.g.: Aharony, A. In *Directions in Condensed Matter Physics*; Grinstein, G., Mazenko, G., Eds.; World Scientific: Singapore, 1986; Vol. 1, p 1. Zallen, R. *The Physics of Amorphous Solids*; Wiley: New York, 1983. Stauffer, D. *Introduction to Percolation Theory*; Taylor and Francis: London, 1987.

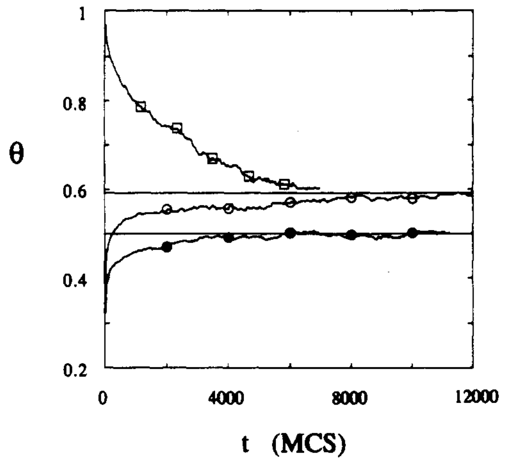

Figure 2. The coverage, θ, as a function of time, t, in the A + B → 0 model without diffusion: (○) on a 500 × 500 square lattice, starting from an initially empty surface (averaged over 35 simulations); (□) on a 500 × 500 square lattice, starting from an almost fully covered surface and fully segregated initial state; (●) on a 250 000 site triangular lattice, starting from an initially empty surface (averaged over 10 simulations). The horizontal lines are the site percolation thresholds (P_c) on square and triangular lattices, respectively.

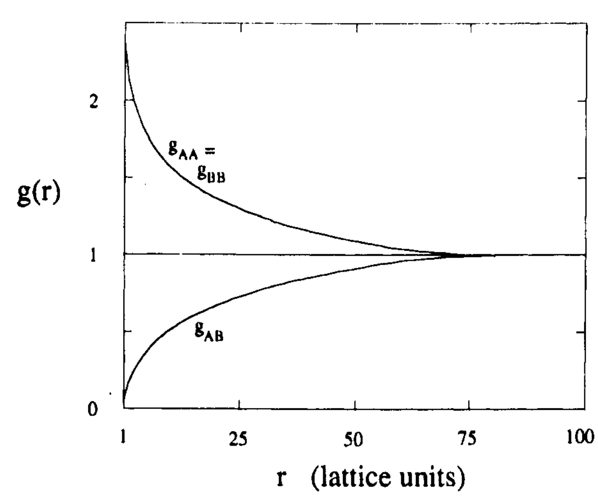

Figure 3. The radial distribution function of a (near) steady-state overlayer generated by the A + B → 0 reaction scheme, with no diffusion (K = 0). The curves correspond to the average of five simulations on a 500 × 500 square lattice.

belongs to an s cluster (in which case it is connected to $s - 1 \sim s$ sites) it follows from (2) and (3) that ξ is a (weight) average distance between sites belonging to the same cluster. Analyzing the results of our simulations on the 500 × 500 square lattice we find $\xi \simeq 90$ lattice units, which is of the same order as the range of correlation (~60) implied by $g_{kl}(r)$. It should be stressed that ξ (and similarly the range of $g(r)$) increases with the system's size L, e.g., for a lattice size $L \times L$ = 100 × 100 we find $\xi \sim 20$. We have not attempted to derive a more quantitative (scaling) relationship between L and ξ, because of the limited range of L values over which the simulations are meaningful. Qualitatively it may be concluded that the range of segregation and correlations is "macroscopic" on the scale of the system analyzed.

2.C. Structural Characteristics. The ramified structure of the A and B islands suggests that they might be fractal objects. This notion was confirmed by Ziff and Fichthorn,[21] for a system with immobile particles. They found that the scaling relation

$$R_s \sim s^{1/D} \qquad (4)$$

between island sizes, s, and the corresponding radii of gyration, R_s, is obeyed with s varying over several orders of magnitude, indicating self-similarity. The fractal dimension obtained was D = 1.90 ± 0.03. This value is essentially identical with the fractal dimension (D = 1.896) characterizing the finite clusters in percolating systems at threshold.[29]

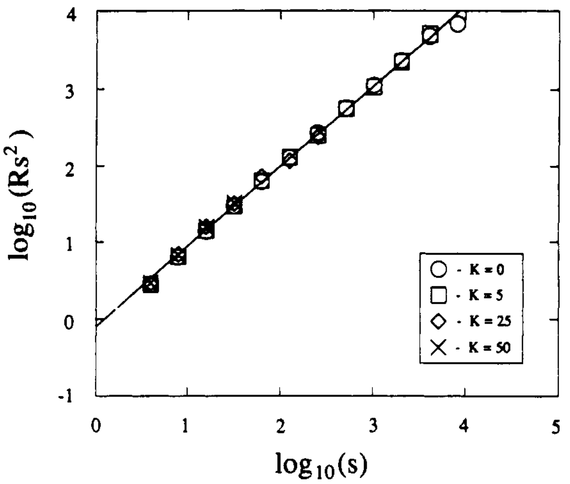

Figure 4. A log-log plot of the gyration radii squared, R_s^2, vs the cluster sizes, s, for several diffusion rates, K = 0 (no diffusion), 5, 25, 50 (on a 500 × 500 square lattice).

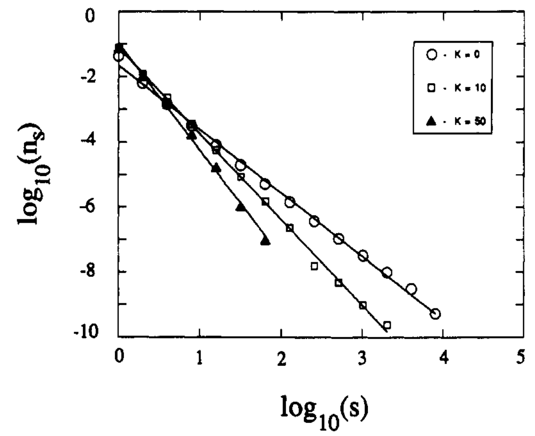

Figure 5. A log-log plot of the cluster size distribution, n_s, vs the cluster sizes, s, for several diffusion rates, K = 0 (no diffusion), 10, 50 (on a 500 × 500 square lattice).

We have repeated the calculation of D, as defined in (4), by analyzing many samples of independent simulations (35 runs on a 500 × 500 square lattice, analyzed after 2000 MCS), and found it to be D = 1.89 ± 0.02, in excellent agreement with ref 21. Figure 4 shows a log-log plot of R_s vs s, demonstrating that (4) is obeyed over several orders of magnitude. Furthermore, the same value of D is found for both smaller (100 × 100 lattices) and larger samples (recall that the lattice size in ref 21 is 1024 × 1024), supporting $D \simeq 1.9$ as the asymptotic value of the fractal dimension.

In addition to the data for immobile reactants (K = 0), Figure 4 shows also the results for systems with different rates of particle diffusion (K = 5–50). It is apparent that the value of D is independent of K (see section 2D).

In percolating systems, at threshold, the size distribution of finite clusters obeys the scaling relation

$$n_s \sim s^{-\tau} \qquad (5)$$

where $\tau = 1 + d/D$, with d denoting the Euclidean dimension of the embedding lattice, and D is the fractal dimension. Thus, for d = 2 and D = 1.9 one expects τ = 2.055. Ziff and Fichthorn[21] tested eq 5 for the AB reactive system (without diffusion, K = 0) and concluded that τ is slightly larger than 2. One cannot rule out that, indeed, τ = 2.055 but the accuracy of the slope of the log n_s vs log s plots does not warrant a more definitive statement. In Figure 5 we show the corresponding plots based on our simulations, both for stationary (K = 0) and mobile ($K > 0$) reactants. We also find that $\tau \gtrsim 2$ for K = 0. However, as K increases τ also increases, indicating that particle diffusion shifts the cluster size distribution to lower sizes (see section 2D). It is also possible, although this is not obvious from the data, that the simple power law dependence (5) does not apply when $K \neq 0$ (similar to the behavior in percolating systems below threshold). In any case, the variation of τ with K should be contrasted with the invariance of D with respect to K; see Figure 4.

We reiterate the two points of similarity between the structure of the A,B overlayer in the A + B → 0 reaction and in percolating systems: (i) The steady-state coverage on the square lattice (for $K = 0$), $\theta^* = \theta_A + \theta_B = 0.59$ is very close to the precolation threshold on this lattice, $P_c = 0.593$. (ii) The fractal dimensions $D \simeq 1.9$ are very similar. To further explore this similarity, we repeated our simulation of the A + B → 0 reaction (for $K = 0$) on a triangular lattice (of 250 000 sites). Here, we found $\theta^* = 0.49$, again just below the percolation threshold, $P_c = 0.50$. For the fractal dimension, which should be independent of the lattice coordination we obtained $D = 1.88 \pm 0.03$, again, in good agreement with the value for the square lattice and that of percolating clusters.

Regardless of the striking similarities of D and of θ^* in the reactive A,B overlayer and percolation systems, it is qualitatively apparent from Figure 1 that the A,B islands are "bulkier" than percolation clusters at the same coverage. In other words, the coastline of the A,B islands appears less tortuous than in percolation clusters. This observation is quantitatively confirmed by comparing the fractal dimension associated with the external perimeter, or the "hull", of the clusters. Following Voss[30] we have calculated the hull dimension, D_h, using the two scaling relations,

$$H \sim \lambda^{D_h} \tag{6}$$

$$H \sim A^{D_h/2} \tag{7}$$

In these equations H is the hull length of the cluster, i.e., the number of all occupied cluster sites which are neighbors of vacant external sites. λ is some linear dimension of the cluster, which may be taken as $(\Delta x \Delta y)^{1/2}$ with Δx (Δy) denoting the length of the projection of the cluster on the x (y) axis. Alternatively, λ may be identified with the radius of gyration R. The cluster area A is defined as the total area confined by the hull (both occupied sites and inner lakes). For percolation clusters both relations yield $D_h = 1.75 \pm 0.01$[30-32] whereas for the A + B system we find $D_h = 1.47 \pm 0.02$, confirming that the edges of percolation clusters are, indeed, considerably more ramified.

Percolation clusters contain many fjords and bays, separated from the outside ocean by narrow straits. If we define a "coarse grained" hull length E as the (shortest) total length of occupied perimeter sites connected via either nearest-neighbor or next-nearest-neighbor sites (in contrast to the hull, H, that is only nn connected), most of these fjords and bays will not contribute to E, corresponding to smoother cluster coastlines. In analogy to (6) or (7), we define D_e via $E \sim \lambda^{D_e}$ and $E \sim A^{D_e/2}$. For percolation clusters we expect D_e to be considerably smaller than D_h, and indeed $D_e = 1.37 \pm 0.03$.[32] On the other hand, for the reactive A,B overlayer we find $D_e = 1.47 \pm 0.03$, which is the same as D_h, indicating the absence of narrow straits in the A,B overlayer.

Another measure employed by us to compare the A,B and percolation clusters is the probability distribution of nearest neighbors, P_n. We define P_n as the fraction of particles with n occupied nearest-neighbor sites; $n = 0, ..., 4$ for the square lattice. Note that in our reactive system A particles cannot have B particles as nearest neighbors, and vice versa. For a percolating system with particle density θ, P_n is the binomial distribution $P_n = [4!/n!(4-n)!]\theta^n(1-\theta)^{4-n}$. In Figure 6 we show P_n for the reactive A + B ($K = 0$) system and for percolation clusters, both for $\theta = 0.55$. The difference is apparent and consistent with the general notion that the A,B clusters are less ramified. In fact, we see that for percolation clusters P_n is maximal for $n = 2$, large for $n = 1$ and 3, and very small for $n = 4$, indicating that most of the sites have vacant neighbors; i.e., most sites belong to the cluster's perimeter. (Note that the dominance of $n = 2$ corresponds to a stringlike structure.) On the other hand, in the A,B system about one-third of the particles belong to the interior ($n = 4$) of the islands, revealing a higher degree of compactness.

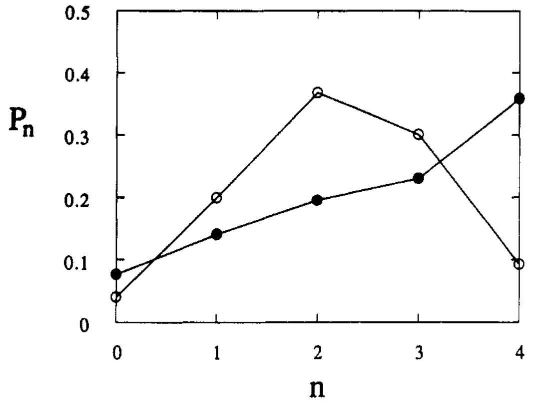

Figure 6. The probability, P_n, that a given adsorbed particle has n occupied nearest-neighbor sites, in the absence of diffusion ($K = 0$): (○) random distribution, (●) the A + B → 0 model (on a 500 × 500 square lattice). For both cases $\theta = 0.55$.

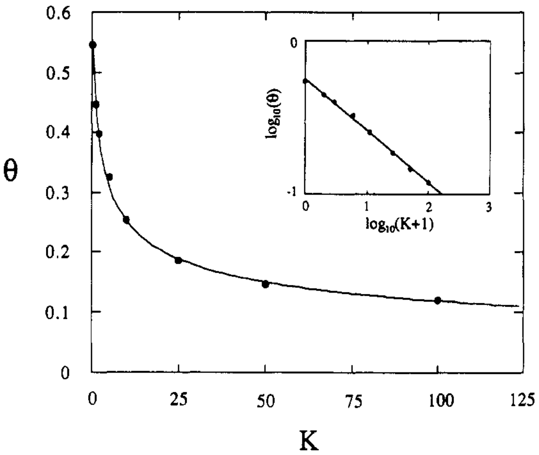

Figure 7. The (near) steady-state coverages, θ^*, in the reactive A + B → 0 system as a function of the diffusion rate, K. The data points are evaluated after 2000 MCS, except for $K = 0$ (12 000 MCS). Insert: A log–log plot of θ^* vs ($K + 1$). (On a 500 × 500 square lattice.)

2.D. Effects of Diffusion. In the absence of diffusion ($K = 0$), reaction takes place only if an A(B) particle has landed on a vacant site neighboring a B(A) occupied site. We will refer to this process as the direct reaction mechanism. If, between successive adsorption events, the adsorbed particles have enough time to perform several (K) diffusion steps and thus visit additional lattice sites, the reaction rate will obviously increase due to the additional ("indirect" or diffusive) route for A + B encounters. Higher reaction rate implies higher adsorption rate, because at steady state these two processes which respectively annihilate and create A,B particles in the system are exactly balanced. Thus, since the rate of adsorption is $J(1 - \theta^*)$ we expect that the steady-state coverage, θ^*, will decrease as K/J increases.

Figure 7 reveals that, indeed, θ^* decreases monotonically with the rate of diffusion K. The slope of the log θ^* vs log ($K + 1$) line shown in the insert is $\alpha \simeq -0.35$. This should be contrasted with the value $\alpha = -0.5$ expected in the limit of very fast diffusion (i.e., very low θ) and classical kinetics. Explicitly, classical reaction kinetics corresponds to reaction rate R, which (apart from a numerical constant of order 1) is given by

$$R = K\theta_A{}^{\chi}\theta_B{}^{\chi} = (K/4)\theta^{2\chi} \tag{8}$$

with reaction order $\chi = 1$ and $\theta = 2\theta_A = 2\theta_B$. At steady state the rates of adsorption, $J(1 - \theta)$, and reaction, R, are equal, and hence $\theta^{2\chi} \sim J(1 - \theta)/K$. In the limit of fast diffusion, $K/J \gg 1$, we find $\theta \ll 1$; hence $\theta \sim K^{\alpha}$ with $\alpha = -(1/2\chi)$, which means

---

[30] Voss, R. F. *J. Phys. A: Math. Gen.* **1984**, *17*, L373.
[31] Ziff, R. M. *Phys. Rev. Lett.* **1986**, *56*, 545.
[32] Grossman, T.; Aharony, A. *J. Phys. A: Math. Gen.* **1986**, *19*, L745.

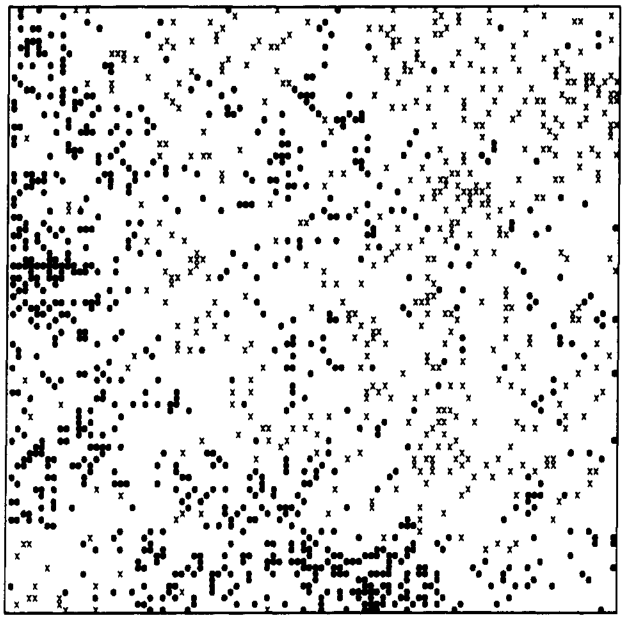

Figure 8. A snapshot of the A,B overlayer, after 2000 MCS, in the presence of surface diffusion ($K = 50$). A 100 × 100 section of the 500 × 500 square lattice used in the calculation is shown.

$\alpha = -1/2$ in the limit of classical kinetics, $\chi = 1$. Thus, the value $\alpha = -0.35$ ($\chi = 1.4$) derived from our simulations corresponds to an anomalously high reaction order. Such, nonclassically high reaction orders have been reported previously for the $A + B \rightarrow 0$ reaction on Sierpinski lattice and other restricted topologies.[10] Qualitatively, in the $A + B \rightarrow 0$ system the reactants are also restricted to diffuse in a restricted region of space, namely in the corridors of the "buffer zone" separating A and B clusters. In this sense, the observation of a high and nonclassical reaction order is not too surprising. However, the origin of this behavior is not at all obvious.

Figure 1 reveals that all A,B islands involve some narrow corridors connecting bulkier regions ("blobs"). Such corridors in A islands are quite easily destroyed by diffusing B's, resulting in fragmentation of the islands into smaller ones. We thus expect that, as K increases (and θ decreases), the average island size decreases as well. This notion is borne out both quantitatively and qualitatively. The qualitative aspect is illustrated in Figure 8 which shows a snapshot of the steady-state overlayer structure for a system with $K = 50$. The smaller island sizes are apparent. The increase of τ with K (cf. (5) and Figure 5) provides a quantitative measure of this trend. Note, however, that although the maximal island size decreases with K, the self-similar character of the islands appears to be preserved, as indicated by the fact that D is independent of K, cf. (4) and Figure 4.

Figure 9 shows P_n, the nearest-neighbor probability distribution, for $K = 50$. Also shown is the binomial distribution $P_n = [4!/n!(4-n)!]\theta^n(1-\theta)^{4-n}$ describing a random (percolation) system at the same total coverage ($\theta = 0.145$), as that of the A,B system. Not surprisingly, at this lower coverage, the two distributions appear much more similar than for the $K = 0$ case (Figure 6). Note, however, that at low coverages when nearest-neighbor pairs are rare (and even more so, triplets and higher clusters) P_n provides little information on the segregation tendency in the system. From Figure 8 it is apparent that, even though the surface is sparsely covered, segregated regions of A's and B's are clearly identifiable.

3. Summary and Conclusions

The rate of change of θ_A in the $A + B \rightarrow 0$ reaction can be expressed as a sum of three contributions: (i) a source term, corresponding to the adsorption of A particles into vacant sites surrounded by either vacant or A-occupied nn sites (otherwise, i.e., if one or more of the nn sites is occupied by B, the newly adsorbed A will react instantaneously with one of them). The rate of this process is $J_A(1-\theta)P_z(\neq B|0)$ with $P_z(\neq B|0)$ denoting the probability that none of the z nearest neighbors of the vacant site (where A has landed) is occupied by B. (ii) A direct reaction term corresponding to the adsorption of a B particle into a vacant site with at least one occupied by A. This process reduces θ_A with a rate given by $J_B(1-\theta)[1-P(\neq A|0)]$. (iii) An indirect, or diffusion limited, reactive term corresponding to reaction following the migration of adsorbed A's and B's toward each other. The rate of this process is given by $Kf(\{A,B\})$ with K denoting the diffusion rate and $f(\{A,B\})$ is some (unknown) function of the lateral distribution, $\{A,B\}$, of the adsorbates on the surface. We thus have

$$d\theta_A/dt = J_A(1-\theta)P_z(\neq B|0) - J_B(1-\theta)[1-P_z(\neq A|0)] - Kf(\{A,B\}) \quad (9)$$

A similar equation (with A and B exchanged) describes $d\theta_B/dt$. Subtracting the two equations we find $d(\theta_A - \theta_B)/dt = (J_A - J_B)(1-\theta)$ revealing, as expected, that if $J_A > J_B$ the surface will be eventually poisoned by A, etc. Thus, a necessary condition for a steady state with finite coverage, $\theta^* < 1$, is that $J_A = J_B = J$. In this case we have of course $\theta_A = \theta_B = \theta/2$ and $P_z(\neq B|0) = P_z(\neq A|0)$, and (9) becomes

$$d\theta/dt = J(1-\theta)[2P_z(\neq A|0) - 1] - 2Kf(\{A,B\}) \quad (10)$$

Considering the complex patterns of the A,B adlayer described in the previous section, it is highly nontrivial to derive closed form expressions for $P_z(\neq A|0)$, or $f(\{A,B\})$. Thus, simple solutions either in closed form or in numerical form can only be obtained for special cases and subject to rather drastic approximations. One particular case of interest which we have studied in detail in the previous section corresponds to the limit of zero adsorbate mobility $K = 0$. In this case, we find from (10) that a steady state ($d\theta/dt = 0$) with finite coverage is achieved if $P_z(\neq A|0) = 1/2$. The simplest possible approximation of P_z corresponds to assuming (as in the Bragg-Williams, "mean-field", scheme) that the sites are randomly populated. In this approximation the probability that any given site is not populated by A is $1 - \theta_A = 1 - \theta/2$, and hence $P_z(\neq A|0) = (1 - \theta/2)^z$. For the steady-state coverage we find in this approximation

$$\theta^* = 2[1 - 1/2^{1/z}] \quad (11)$$

which yields $\theta^* = 0.32$ and 0.22 for the square ($z = 4$) and triangular ($z = 6$) lattices, respectively. These values are in poor agreement with the results of the simulations, $\theta^* \simeq 0.59$ and 0.49, respectively.

Another, supposedly better approximation is the analogue of the quasi-chemical scheme, in which pairs of nearest-neighbor sites (as opposed to single sites) are treated as independent.[18] In this case one writes $P_z(\neq A|0) = [1 - P(A|0)]^z$, where $P(A|0)$ is the conditional probability that a site neighboring a vacant site will be occupied by A. The conditional probabilities are related to the pair occupation probabilities via $P(i|j)\theta_j = P(i,j)$ with i, j =

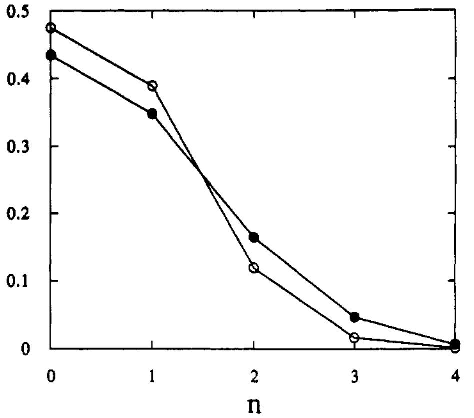

Figure 9. The probability, P_n, that a given adsorbed particle has n occupied nearest-neighbor sites, in the presence of diffusion ($K = 50$): (○) random distribution, (●) the $A + B \rightarrow 0$ model (on a 500 × 500 square lattice.) For both cases $\theta = 0.145$.

4810 J. Phys. Chem. 1991, 95, 4810-4813

A, B, or 0. Rate equations can be written for the pair and singlet probabilities and solved numerically for the steady-state values of these quantities.[18] The results obtained for θ^* through this higher order approximation are very similar to those derived from the site approximation. The fact that the pair approximation does not improve significantly the singlet approximation is not very surprising in view of the long-range correlations demonstrated by the results of the simulations. Site, pair, or higher cluster approximations can also be written and solved for systems with finite diffusion rate ($K \neq 0$). However, since the size of the cluster *defines the range of correlations accounted for by the model, it* is clear that such schemes cannot explain the complex island structures and unusual reaction rates revealed by the computer experiments.

Several authors have formulated analytical approaches starting out with the rate equations for the local densities of the reactive adsorbates.[13,14] Based on these equations one can analyze the steady-state behavior of various correlation functions and order parameters which measure the extent of reactant aggregation and segregation. For simple reaction rate and diffusion laws, such treatments can yield considerable insight regarding the relation between segregation and dimensionality (see section 1), and about the interplay between the rates of diffusion, reaction, and particle deposition. Yet, because of their continuous ("coarse grained") nature they cannot provide detailed structural information on, say, the overlayer characteristics in the $A + B \rightarrow 0$ reaction on a lattice. In some cases the predictions of such models are in conflict with the results of simulation studies. For instance, in ref 14 it is concluded that a finite diffusion rate is necessary to promote A,B segregation, because otherwise the distribution of A and B on the surface will be random, reflecting the uncorrelated deposition of A and B by the source. This behavior is of course in marked contrast to our simulations which show macroscopic segregation even for $K = 0$.

We conclude this paper with the notion that even a very simple and familiar system, such as the $A + B \rightarrow 0$ reaction on a surface, can exhibit complex and rich behavior and present some puzzling questions. These questions pertain in particular to the possible relation between the A,B clusters and percolating systems at threshold. The appearance of similarities is not unreasonable in view of the fact that, apart from the restriction that A's and B's are not allowed to nearest-neighbor sites, their distribution is (apparently) random, as in percolation systems. However, whether a rigorous analogy between the $A + B \rightarrow 0$ and the percolation problem does or does not exist is still an open question.

Acknowledgment. This research was partly supported by grants from the VDI Düsseldorf, Germany, the National Council for Research and Development, Israel, and the Fund for Basic Research administered by the Israel Academy of Sciences. The Fritz Haber Research Center is supported by the Minerva Gesellschaft für die Forschung, mbH, Munich, BRD. We thank the referees for drawing our attention to the very recent work described in ref 14b.

On the Problem of Reaction Site in Biphasic Extraction of Metal Ions: NMR versus Spectrophotometric Evidence in Micellar Model Systems

C. Tondre* and D. Canet

Laboratoire d'Etude des Solutions Organiques et Colloidales (LESOC), Unitê Associêe au CNRS No. 406, Universitê de Nancy I, B.P. 239, 54506 Vandoeuvre-lês-Nancy Cedex, France *(Received: August 1, 1990)*

A much debated question in solvent extraction is that of the locale of the metal–extractant reaction: in the homogeneous aqueous phase or the organic/aqueous interface? Due to the existence of microscopic interfaces, micellar solutions and microemulsions can serve as model systems to try answering this question. Taking advantage of the very slow rate of complexation between an alkylated derivative of 8-hydroxyquinoline and Ni^{2+} in CTAB/butanol micelles, we were able to make use of NMR as well as UV–visible spectrophotometry for kinetic investigations. Whereas UV–visible spectroscopy directly monitors complex formation, NMR spectroscopy has permitted us to detect the interaction of Ni^{2+} with the surface of CTAB/butanol micelles in which the extractant is solubilized. Kinetic data obtained from both techniques turn out to be identical, tending to demonstrate that, viewed from the micelles, the reaction takes place at the microscopic interface. Critical examination shows that the answer might not be so simple.

Introduction

During the last few years, a large amount of work in the field of solvent extraction has been devoted to the problem of the locale of the rate-limiting metal–extractant reaction.[1-10] Such reactions are usually carried out in biphasic heterogeneous systems, with a lipophilic extractant dissolved in an organic phase and the metal ions solubilized in an aqueous phase. When the reaction takes place in a stirred reactor, different regimes can be distinguished depending on the stirring rate.[11] At low rates, the kinetics is dominated by the diffusion of the reagents in the stagnant layers surrounding each particle of the dispersed phase. At high stirring rate, a kinetic regime sets up and the proper complexation step becomes rate-limiting.

A much debated point concerns the reaction site, which can be either the homogeneous aqueous phase or the organic/aqueous

---

(1) Szymanowski, J.; Prochaska, K. *J. Radioanal. Nucl. Chem.* **1989**, *129*, 251.
(2) Chamupathi, V. G.; Freiser, H. *Inorg. Chem.* **1989**, *28*, 1658.
(3) Osseo-Asare, K. *Colloids Surf.* **1988**, *33*, 209.
(4) Albery, W. J.; Choudhery, R. A. *J. Phys. Chem.* **1988**, *92*, 1142.
(5) Freiser, H. *Bull. Chem. Soc. Jpn.* **1988**, *61*, 39; *Chem. Rev.* **1988**, *88*, 611.
(6) Watarai, H.; Takahashi, M.; Shibata, K. *Bull. Chem. Soc. Jpn.* **1986**, *59*, 3469.
(7) Szymanowski, J. *Polyhedron* **1985**, *4*, 269.
(8) Osseo-Asare, K. In *Hydrometallurgical Process Fundamentals*; Bautista, R. C., Ed.; Plenum: New York, 1984.
(9) Akiba, K.; Freiser, H. *Anal. Chim. Acta* **1982**, *136*, 329.
(10) Danesi, P. R.; Vandegrift, G. F.; Horwitz, E. P.; Chiarizia, R. *J. Phys. Chem.* **1980**, *84*, 3582.
(11) Danesi, P. R.; Chiarizia, R. *Crit. Rev. Anal. Chem.* **1980**, *10*, 1-126.